Effect of sound on gap-junction-based intercellular signaling: Calcium waves under acoustic irradiation

P. A. Deymier,[1,*] N. Swinteck,[1] K. Runge,[1] A. Deymier-Black,[2] and J. B. Hoying[3]
[1]*Department of Materials Science and Engineering, University of Arizona, Tucson, Arizona 85721, USA*
[2]*Department of Orthopaedic Surgery, Washington University in St. Louis, St. Louis, Missouri 63110, USA*
[3]*Cardiovascular Innovation Institute, University of Louisville, Louisville, Kentucky 40202, USA*
(Received 9 June 2015; revised manuscript received 11 August 2015; published 9 November 2015)

We present a previously unrecognized effect of sound waves on gap-junction-based intercellular signaling such as in biological tissues composed of endothelial cells. We suggest that sound irradiation may, through temporal and spatial modulation of cell-to-cell conductance, create intercellular calcium waves with unidirectional signal propagation associated with nonconventional topologies. Nonreciprocity in calcium wave propagation induced by sound wave irradiation is demonstrated in the case of a linear and a nonlinear reaction-diffusion model. This demonstration should be applicable to other types of gap-junction-based intercellular signals, and it is thought that it should be of help in interpreting a broad range of biological phenomena associated with the beneficial therapeutic effects of sound irradiation and possibly the harmful effects of sound waves on health.

DOI: 10.1103/PhysRevE.92.052711 PACS number(s): 87.50.Y−, 87.17.Aa, 87.18.Gh

I. INTRODUCTION

The interactions between sound waves and living tissue were first observed and reported in the early 20th century [1,2]. Since then ultrasound-based therapies have been used to treat a very wide range of medical disorders [3]. Ultrasound stimulation accelerates the bone fracture repair process [4,5]. Therapeutic ultrasound is also commonly employed to manage soft tissue lesions [6]. The ability of ultrasound to focus through the skull noninvasively has lately made it an attractive technique for neuromodulation to treat neurological disorders [7]. More recently, ultrasound has also been shown to remove amyloid plaque and restore memory in an Alzheimer's disease mouse model [8]. The therapeutic benefits of high-intensity sound irradiation have been associated to date with thermal effects such as local heating due to absorption of sound energy by the tissue, and also with nonthermal effects [9]. Physical effects other than temperature in fluid-containing tissues include cavitation leading to concentration of the delocalized sound wave energy into high-energy gaseous bubbles and acousto-hydrodynamics phenomena such as streaming or microstreaming. In the case of low-intensity ultrasound irradiation, mechanical effects resulting from the pressure field of the sound wave may induce mechano-transduction processes such as transient elevation of intracellular calcium in bone cells [10]. In addition, the acoustic pressure in solid tissue may lead to tension in cell membranes and alter membrane conductance [11]. Reversible suppression of transmission of cortical potentials along neural pathways was achieved by ultrasound irradiation [12]. A significant increase in gap junctional cell-to-cell communication in rat bone marrow stromal cells subjected to low-intensity ultrasound irradiation was demonstrated [13]. There is also evidence that ultrasound modulates the ionic conductance of neurons and astrocytes and can stimulate electrical activity and calcium signaling in mice hippocampal slice cultures and *ex vivo* brains [14].

Here, we present a previously unrecognized effect of sound waves on biological tissue and in particular, on gap-junction-based intercellular signaling. The purpose of this paper is to demonstrate a possible mechanism by which a sound wave can modulate spatially and temporally the conductance between cells and impart the property of nonreciprocity in propagation to an intercellular wave. Nonreciprocity in the propagation of waves is associated with time-reversal symmetry breaking, nonconventional wave topologies, and topologically robust one-way propagation. To date, these nonconventional properties have only been described and observed in physical waves such as electronic, electromagnetic, and acoustic waves in systems such as topological insulators [15–17]. We suggest that sound irradiation of some biological tissues may create intercellular waves with nonconventional topologies that can lead to unidirectional signal propagation. We illustrate this mechanism in the case of an intercellular calcium wave. Calcium and calcium waves are biological regulators of differentiation and activity in numerous tissue types [18–22]. The mechanisms of initiation and propagation of intercellular calcium waves may involve cell-to-cell communication with intracellular messengers diffusing through gap junctions or extracellular messengers mediating paracrine signaling [23]. Intercellular calcium waves in tissues composed of endothelial cells originate from (a) feedback loops between Ca^{2+} and the messenger molecule inositol 1,4,5-triphosphate IP_3 [24–26] and (b) cell-to-cell interactions via Ca^{2+} and IP_3 transport through gap junctions [27,28]. In other tissues, cell-to-cell communication can circumvent the gap-junction pathway, involving other mechanisms such as paracrine signaling via extracellular messengers.

Turing noted the importance of studying the behavior of biological processes by considering the complementarity of both linear and nonlinear dynamical systems [29]: "Such systems (*with linear dynamics*) certainly have a special interest as giving the appearance of a pattern, but they are the exception rather than the rule. Most of an organism, most of the time, is developing from one pattern into another, rather than from homogeneity into a pattern. One would like to be able to follow this more general process (*nonlinear*) mathematically

*Corresponding author: deymier@email.arizona.edu

also. The difficulties are, however, such that one cannot hope to have any very embracing *theory* of such processes, beyond the statement of the equations. It might be possible, however, to treat a few particular cases in detail with the aid of a digital computer." Therefore we address the interaction between acoustic waves and calcium waves from a theoretical point of view using a linear reaction-diffusion model for the calcium dynamics in multicellular tissues, as well as from a computational point of view in the case of a more complex and biologically realistic nonlinear reaction-diffusion model.

In Sec. II A, the effect of acoustic irradiation on calcium signaling is investigated computationally in the case of a nonlinear intracellular calcium dynamics. We set out to develop a computational model of nonlinear intercellular calcium waves propagating along a numerically tractable prototypical tissue taking the form of a chain of cells that may be composed of endothelial cells. We employ a nonlinear reaction-diffusion model to describe the spatiotemporal behavior of the Ca^{2+}-IP_3 coupling in that tissue. An acoustic wave that affects the gap-junction conductance is shown to break the reciprocity in the direction of propagation of trains of nonlinear calcium waves. In Sec. II B, we then analyze theoretically this numerical model whereby the reaction dynamics is linearized. Within the context of linear dynamics, the system is considered to be not very far from a homogeneous equilibrium. Using multiple time scale perturbation theory, we show that subjecting a tissue composed of endothelial cells to an acoustic wave leads to symmetry breaking of the calcium wave which then exhibits a nonconventional topology. In the third and final section, conclusions are drawn. We note that the observed mechanism of nonreciprocity in the intercellular calcium wave propagation should be applicable to other types of gap-junction intercellular signals. Furthermore, we discuss the sensitivity of the observed nonreciprocity in the propagation of calcium signals to the biological complexity of the models. We also focus on the relevance of the present theoretical and computational demonstration of existence that sound irradiation can break symmetry in the direction of propagation of gap-junction-based intercellular calcium signals.

II. MODELS, METHODS, AND RESULTS

A. Nonlinear reaction-diffusion model of gap-junction-based intercellular calcium waves

This section is devoted to the particular case of a nonlinear reaction-diffusion model of calcium waves and on the effect of an acoustic wave on the propagation of gap-junction-based intercellular signals. The model of nonlinear calcium waves involves primarily the nonlinear intracellular reaction dynamics coupled with the intercellular diffusion of cytoplasmic calcium and IP_3. The intracellular chemical reaction process is based on a model introduced by Politi *et al.* [30]. A schematic of this intracellular calcium pathway in the context of a multicellular structure with intercellular gap-junction diffusion is shown in Fig. 1. The complete reaction-diffusion process involves primarily the intracellular reaction dynamics and the intercellular diffusion of cytoplasmic calcium and IP_3. For the sake of completeness, we describe this model in some detail. The intracellular calcium pathway starts with an

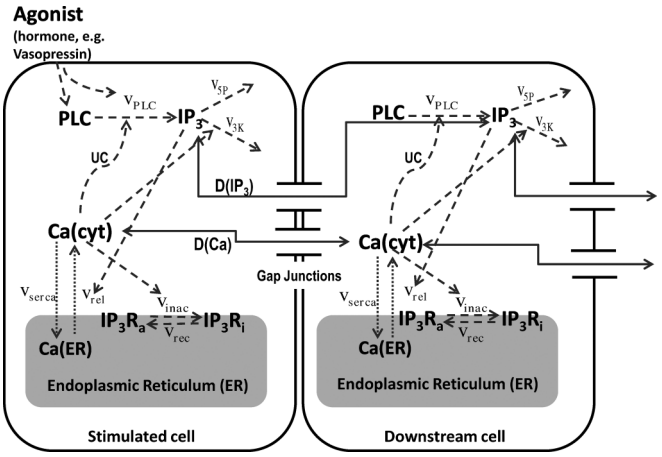

FIG. 1. Reaction-diffusion process of Ca^{2+} and IP_3 metabolism included in the nonlinear model (after Ref. [30]). The solid, dashed, and dotted arrows indicate molecular diffusion, regulatory interactions, and reaction-transport steps, respectively. The bold quantities indicate the following model variables: IP_3, the cytoplasmic IP_3: Ca(*cyt*), the free cytoplasmic Ca^{2+}; Ca(*ER*), the free Ca^{2+} in the ER; IP_3R_a, the active conformation of the IP_3R. The other abbreviations denote IP_3R_i, the inactive conformation of the IP_3R; v_{serca}, the active Ca^{2+} transport into the ER; v_{PLC}, the production rate of IP_3; v_{rel}, the rate of Ca^{2+} release through the IP_3R; v_{inac} and v_{rec}, the rates of Ca^{2+}-induced IP_3R inactivation and recovery, respectively; v_{5P} and v_{3K}, the rates of IP_3 dephosphorylation and phosphorylation, respectively; D(IP_3) and D(*Ca*), the gap-junction diffusion coefficient of IP_3 and Ca, v_{serca} respectively; and *UC*, the threshold of Ca needed to activate PLC.

extracellular agonist that combines with the G-protein-coupled receptors on the cell's membrane to activate phospholipase C (PLC). It is, in turn, able to catalyze the production of IP_3 [31]. IP_3 then can bind to the IP_3 receptor, IP_3R, to open calcium channels in the membrane of the endoplasmic reticulum (ER). This process releases stored Ca^{2+} into the cytosol. Meanwhile, the cytoplasmic Ca^{2+} can create both positive and negative feedback conditions in the production of IP_3. For the positive feedback condition, the cytoplasmic Ca^{2+} is capable of activating the PLC isoforms to release more IP_3 [32]. For the negative feedback condition, the increase in cytoplasmic Ca^{2+} can activate the IP_3 degradation via IP_3 3-kinase (IP_3K). Cells subsequently control the intracellular calcium level by buffering, sequestering in specialized compartments, and expelling to the extracellular space excess calcium, thereby maintaining calcium homeostasis and resetting the signaling loop [25,33].

The intracellular chemical reaction dynamics is formulated into a system of coupled differential equations involving four dynamical variables: the calcium concentration in the cytosol, c; the IP_3 concentration in the cytosol, p; the calcium concentration in the ER stores, s; and the fraction of IP_3R that has not been inactivated by Ca^{2+}, r. The rate equation for the IP_3 concentration takes the following form:

$$\frac{dp}{dt} = f(c,p) = v_{\mathrm{PLC}} - v_{\mathrm{deg}} = v_{\mathrm{PLC}} - (v_{5P} + v_{3K})$$
$$= \left(V_{\mathrm{PLC}} \frac{c^2}{K_{\mathrm{PLC}}^2 + c^2}\right) - \left(k_{5P} + k_{3K} \frac{c^2}{K_{3K}^2 + c^2}\right) p, \quad (1)$$

where the v_{PLC} and v_{deg} represent the production and degradation rate of IP_3, respectively. V_{PLC} is the maximum production rate of PLC that depends on the agonist concentration. K_{PLC} characterizes the sensitivity of PLC to Ca^{2+}. Phosphorylation and dephosphorylation lead to degradation of IP_3 with the rates v_{3K} and v_{5P}, respectively. The phosphorylation rate is described by a Hill function with the rate constant k_{3k} and the half-saturation constant K_{3K} [34].

The rate equation for the cytoplasmic Ca^{2+} takes the following form:

$$\frac{dc}{dt} = g(c,p) = v_{\mathrm{rel}} - v_{\mathrm{serca}} = \left[k_1\left(r\frac{c}{K_a + c}\frac{p}{K_p + p}\right)^3 + k_2\right](s - c) - V_{\mathrm{serca}}\frac{c^2}{K_{\mathrm{serca}}^2 + c^2}. \quad (2)$$

v_{serca} represents the rate for the active Ca^{2+} transport into the ER and v_{rel}, the rate of Ca^{2+} release through the IP_3R. V_{serca} and K_{serca} are the maximum sarcoplasmic-endoplasmic reticulum Ca^{2+}-ATPase (SERCA) pump rate and half-activation constant, respectively.

For the sake of simplicity, the total calcium concentration in the cell c_{tot} is assumed to be conserved and is represented as $c_{\mathrm{tot}} = c + \beta s$, where β is the ratio of effective cytoplasmic volume to effective ER volume (both accounting for Ca^{2+} buffering). Therefore the calcium concentration in the ER store can be expressed as

$$s = \frac{c_{\mathrm{tot}} - c}{\beta}. \quad (3)$$

The dynamics of IP_3R inactivation by Ca^{2+} is modeled as follows:

$$\frac{dr}{dt} = v_{\mathrm{rec}} - v_{\mathrm{inac}} = \frac{1}{\tau_r}\left(1 - r\frac{K_i + c}{K_i}\right). \quad (4)$$

v_{inac} and v_{rec} are the rates of Ca^{2+}-induced IP_3R inactivation and recovery, respectively.

The simulation of intracellular oscillations reported herein uses the model parameters reported by Politi [30]. Reference [30] extensively discusses the physiological role of both positive and negative Ca^{2+}-IP_3 feedbacks in relation to the enhancement of the range of frequency encoding of the agonist stimulus. However, since the frequency encoding supported by the positive feedback appears to be more robust against variations in the parameters describing the calcium kinetics, we have limited ourselves to the model supporting calcium positive feedback. Positive feedback is achieved in the model by setting the phosphorylation rate constant k_{3k} to zero. We anticipate that the effect of an acoustic wave on Ca^{2+} signal propagation in a multicellular structure does not depend qualitatively on this choice since, as will be seen below, the acoustic wave impacts the cell-to-cell conductance. All the parameters of the model are summarized in Table I. The numerical solutions of Eqs. (1), (2), and (4) are obtained by using a fourth-order Runge-Kutta algorithm with time step size, $\Delta t = 0.01$ s.

Politi's model of intracellular calcium pathway is integrated into a multicellular model by considering the phenomenon

TABLE I. Values of parameters used in the nonlinear reaction-diffusion model.

Parameters	Description	Value
	IP_3 dynamics parameters	
K_{3K}	Half-activation constant of IP_3K	0.4 μM
k_{3K}	IP_3 phosphorylation rate constant	0
k_{5P}	IP_3 dephosphorylation rate constant	0.66 s^{-1}
K_{PLC}	Half-activation constant of PLC	0.2 μM
V_{PLC}	Maximum production rate of IP_3	1.5 μM s^{-1}
	Ca^{2+} transport and structural parameters	
β	Ratio of effective volumes ER/cytosol	0.185
V_{serca}	Maximal SERCA pump rate	0.9 μM s^{-1}
K_{serca}	Half-activation constant	0.1 μM
c_{tot}	Total Ca^{2+} concentration	2 μM
	IP_3R parameters	
k_1	Maximal rate of Ca^{2+} release	1.11 s^{-1}
k_2	Ca^{2+} leak	0.0203 s^{-1}
K_a	Ca^{2+} binding to activating site	0.08 μM
K_i	Ca^{2+} binding to inhibiting site	0.4 μM
K_p	IP_3 binding	0.13 μM
τ_r	Characteristic time IP_3R inactivation	12.5 s
	Reference diffusion parameters	
D_c^*	Diffusion coefficient rate of Ca^{2+}	0.005 s^{-1}
D_p^*	Diffusion coefficient rate of IP_3	$10D_c^*$
UC	Threshold of Ca^{2+} to activate PLC	0.057 μM

of diffusion via the gap junction of both Ca^{2+} and IP_3 driven by the concentration gradients between neighboring cells. The multicellular structure considered here is composed of a single linear chain of N cells with periodic boundary conditions (PBC). In developing this model, we have in mind blood vessels where the endothelial monolayer is in reality a two-dimensional structure (wrapped in a tube) which, in the case of capillaries, may be approximated by a one-dimensional chain of endothelial cells, since the cross section approaches the cell dimension. In such a chain, in which every cell is connected to two other cells (diffusion between nearest-neighbor cells), one can write the one-dimensional time-dependent reaction/diffusion equation for Ca^{2+} and IP_3:

$$\frac{\partial c}{\partial t} = D_c\frac{\partial^2 c}{\partial x^2} + g(c,p) = D_c^*[c(x_{i+1},t_n) - 2c(x_i,t_n) + c(x_{i-1},t_n)] + g(c,p) \quad (5)$$

and

$$\frac{\partial p}{\partial t} = D_p\frac{\partial^2 p}{\partial x^2} + f(c,p) = D_p^*[p(x_{i+1},t_n) - 2p(x_i,t_n) + p(x_{i-1},t_n)] + f(c,p), \quad (6)$$

where D_c and D_p are again the diffusion coefficients of Ca^{2+} and IP_3, and x and t are the position and time variables. Equations (5) and (6) have been discretized in space and time using finite differences, and $t_n = n\Delta t$ refers to the discretized time line with the time step Δt. $D_c/\Delta x^2$ and $D_p/\Delta x^2$ are defined as the diffusion coefficient rate of Ca^{2+} and IP_3 with unit per second s^{-1}, which we denote D_c^* and D_p^*, respectively. Δx is the nearest-neighbor cell-center to cell-center distance. Since diffusion occurs via gap junctions, we can assume that

it is limited to nearest-neighboring cells. We further assume that the distribution of gap junctions in the plasma membrane is spatially uniform and that the diffusion coefficients are constants independent of cell number. Note that the mobility of Ca^{2+} through the gap junction is restricted in comparison to that of IP_3 because of the higher buffering capacity of cytoplasm for Ca^{2+} than for IP_3 [35]. Thus IP_3 diffuses much faster than Ca^{2+} [36]. For the sake of simplicity, we set $D_p^* = 10D_c^*$ in our model. We have verified that our combined reaction-diffusion algorithm has fully converged for the time step $\Delta t = 0.01$ s.

To induce trains of calcium waves in the multicellular one-dimensional chain, we initially stimulate a single cell in the center of the chain with the agonist. PLC of the stimulated cell is activated initially by the extracellular agonist to induce intracellular Ca^{2+}-IP_3 oscillations. All other cells in the chain are not initially stimulated ($V_{PLC} = 0$). The reaction dynamics of the stimulated cell increases its calcium concentration. Diffusion of Ca^{2+} between the stimulated cell and its neighboring cells elevates their Ca^{2+} concentration. We enable the propagation of a train of calcium waves by introducing a threshold based on the calcium concentration for inducing Ca^{2+}-IP_3 positive feedback in the neighboring cells (Fig. 1). When the cytoplasmic Ca^{2+} concentration reaches a value exceeding a threshold UC, the positive feedback of cytoplasmic Ca^{2+} is activated to increase the production rate of IP_3. If the cytoplasmic Ca^{2+} concentration is below the threshold, PLC enzymes are not activated. The introduction of this threshold enables the synchronized development of collective spatiotemporal response of the multicellular architecture. This extension is based not only on diffusion but also on an additional amplification mechanism through the generation of IP_3 and the Ca^{2+}-dependent activation of PLC [37]. The general behavior of this nonlinear reaction-diffusion model of calcium wave propagation and the numerical methods for solving the nonlinear coupled differential equations have been detailed in Ref. [38].

In the example case, the model one-dimensional tissue is composed of a chain of 401 cells. Initially, an intracellular calcium oscillation is induced by an extracellular agonist in cell 201. In Fig. 2 (top), we present snapshots (at the same time step = 30 000 Δt) of the nonlinear calcium waves propagating in the absence of acoustic irradiation. In this case, the nonlinear calcium wave takes the form of two trains of pulses propagating symmetrically from the stimulated cell (201). The important feature here is that the calcium waves in the absence of an acoustic wave are symmetric in space and time. This feature is characteristic of reciprocal propagation of the intercellular signals.

We now consider the case of the model tissue subjected to an acoustic wave propagating from the left to the right of the chain of cells. Let us consider a sound wave with a frequency Ω and a wave number K, with the spatially and temporally varying pressure field given by $P(x,t) = P_0 \cos(Kx + \Omega t)$. Here the wave number is $K = \frac{2\pi}{L}$, with L being the wavelength of the sound wave. This pressure field may lead to a modification [13] and modulation of the gap-junction cell-to-cell conductance; however, we need to identify its functional form. It has been shown that gap junctional conductance of Hensen cells is correlated with membrane strain [39]. In that study, experimental data demonstrated a nearly linear relation between the

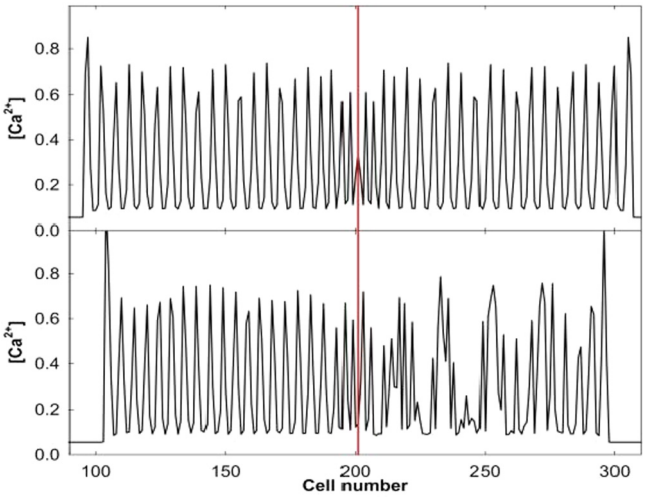

FIG. 2. (Color online) Sound irradiation breaks the reciprocity of nonlinear calcium waves. (Top) Snapshot of the concentration of cytosolic calcium [Ca^{2+}] at time $t = 30{,}000\,\Delta t$ ($\Delta t = 0.01$ s) resulting from the stimulation of cell 201 (red line) in the absence of acoustic irradiation. (Bottom) Snapshot of the concentration of cytosolic calcium at the same time in the presence of acoustic irradiation. Periodic boundary conditions are used, but the simulation is interrupted before the calcium wave can reach cells 1 and 401. The concentrations are in units of μM.

transjunctional conductance and membrane strain up to values of 1.3. Considering a linear Hooke's-law-type relation between pressure and membrane strain and a linear strain-conductance relationship, one expects a linear relation between pressure and gap junctional conductance. Therefore, when subjected to sound irradiation, the spatially and temporally varying diffusion coefficients of the Ca^{2+} and IP_3 are chosen to take a functional form given by the following equations:

$$D_c(x,t) = D_{0c} + 2D_{1c}\cos(Kx + \Omega t), \tag{7a}$$

$$D_p(x,t) = D_{0p} + 2D_{1p}\cos(Kx + \Omega t), \tag{7b}$$

where D_{0c} and D_{0p} are the diffusion constants in the absence of the sound wave that were used in the absence of acoustic irradiation. D_{1c} and D_{1p} reflect the variation in membrane conduction due to a given level of the maximum acoustic pressure. The cosine function in Eqs. (7a) and (7b) parallels the cosine functional form of the pressure wave. When considering spatially and temporally dependent diffusion coefficients, Eqs. (5) and (6) take the form

$$\begin{aligned}\frac{\partial c}{\partial t} &= D_c^*(x_i,t)[c(x_{i+1},t_n) - 2c(x_i,t_n) + c(x_{i-1},t_n)] \\ &\quad + \frac{1}{2}[D_c^*(x_{i+1},t) - D_c^*(x_{i-1},t)] \\ &\quad \times \frac{1}{2}[c(x_{i+1},t) - c(x_{i-1},t)] + g(c,p), \\ \frac{\partial p}{\partial t} &= D_p^*(x_i,t)[p(x_{i+1},t_n) - 2p(x_i,t_n) + p(x_{i-1},t_n)] \\ &\quad + \frac{1}{2}[D_p^*(x_{i+1},t) - D_p^*(x_{i-1},t)] \\ &\quad \times \frac{1}{2}[p(x_{i+1},t) - p(x_{i-1},t)]f(c,p).\end{aligned}$$

The second terms in the right-hand sides of the preceding equations are advective terms involving products of the gradient in composition with the gradient in diffusion coefficient. We first neglect these advective terms and simply insert Eqs. (7a) and (7b) into Eqs. (5) and (6). We therefore show below that such advective terms are not necessary for breaking symmetry in the propagation of calcium waves. We will also show in Sec. II B that advective terms are not necessary to achieve symmetry breaking in our simplified linear reaction-diffusion model. We have also conducted numerical calculations with the advective terms and verified that symmetry breaking also occurs. In our numerical calculations we use $\frac{D_{1c}}{D_{0c}} = \frac{D_{1p}}{D_{0p}} = 0.6$. Under these conditions, we have identified the existence of resonant conditions that lead to disruption of the reciprocity in propagation of the calcium waves. For instance, in the case of irradiation by an acoustic wave with $L = 36\Delta x$ and $\Omega = 7 \times 10^{-3}$ rad/s, Fig. 2 (bottom) shows clearly that the symmetry of the trains of calcium pulses is broken. The train of pulses propagating toward the left retains its integrity although with a reduced wavelength (interpeak distance). In contrast, the calcium wave propagation to the right has completely lost its integrity. Pulses are still propagating but without a well-defined wavelength. In the presence of directed acoustic irradiation, nonreciprocal propagation of nonlinear intercellular calcium waves is therefore observed. For a typical intercellular spacing, $\Delta x \sim 30$ μm, the conditions at which symmetry breaking is observed correspond to a wavelength of $L = 1.08$ mm (a wave number $K = 5.817\,\mathrm{rad/mm^{-1}}$). This condition cannot be realized with a monochromatic sound wave for which the relation $\Omega = cK$ with $c \sim 1500$ m/s would hold. In the previous relation, we take the speed of sound in the biological medium to be that in water. The condition for symmetry breaking can be achieved as the low-frequency beat that arises from the interference resulting from the superposition of two waves that are traveling in opposite directions, namely, $\sin(k_1x + f_1t) + \sin(k_2x - f_2t) = 2\sin[(\frac{k_1+k_2}{2})x + (\frac{f_1-f_2}{2})t]\cos[(\frac{k_1-k_2}{2})x + (\frac{f_1+f_2}{2})t]$. The two waves have slightly different frequencies, f_1 and f_2, and wave numbers, k_1 and k_2, but they both travel with the same wave speed, c. The envelope of the superposition of waves given by the sine function in the right–hand side of the preceding equation will have a wave number comparable to those of the superposed waves. Even if the frequencies f_1 and f_2 are reasonably high, the envelope will impact the gap-junction cell-to-cell conductance with the low beat frequency $\Omega = {}^1\!/_2(f_1\text{-}f_2)$. With wave numbers $k_1 \sim k_2 \sim 5.817\,\mathrm{rad/mm^{-1}}$ and the speed of sound of $c \sim 1500$ m/s, both slightly differing frequencies f_1 and f_2 are on the order of 1.5 MHz, which is typical of sonographic instruments which operate in the range of 1–18 MHz. A plausible scenario that would lead to the condition for symmetry breaking may consist of the interference due to multiple reflections of an incident ultrasonic beam with central frequency of 1.5 MHz with even narrow bandwidth.

Our model shows numerically the phenomenon of nonreciprocity in calcium wave propagation induced by sound wave irradiation. To gain further insight into this phenomenon from a theoretical point of view, we consider in the next section a simplified analytical model to describe the interaction between an acoustic wave and a linearized version of the reaction-diffusion model.

B. Linear reaction-diffusion model of calcium waves

Following Turing's seminal work on linear diffusion-reaction models for modeling morphogenesis [29], we employ a linear reaction-diffusion model to describe the spatiotemporal behavior of the Ca^{2+}-IP_3 coupling in tissues composed of endothelial cells. Similarly to Turing, we assume that the system is not very far from a homogeneous equilibrium and that the linear model describes small variations in composition about that equilibrium. The matter of the multicellular chain is assumed to be continuously distributed. Under these conditions, the dynamics of the small excursions in the concentrations of Ca^{2+} and IP_3 about the equilibrium state, C and P, is described by the linearly coupled set of differential equations:

$$\frac{\partial C(x,t)}{\partial t} = \frac{\partial}{\partial x}\left[D_c(x,t)\frac{\partial C(x,t)}{\partial x}\right] - rP(x,t), \tag{8a}$$

$$\frac{\partial P(x,t)}{\partial t} = \frac{\partial}{\partial x}\left[D_p(x,t)\frac{\partial P(x,t)}{\partial x}\right] + rC(x,t). \tag{8b}$$

This linear model represents a composite regulatory process between Ca^{2+} and IP_3 that leads to effective compositional oscillations. This simplified linear reaction-diffusion model lumps many of the fine-detail control systems of cellular calcium [23] into a single reaction rate constant r. The linear model replaces the functions f and g, by $g(C,P) = aC - rP$; and $f(C,P) = rC + bP$. We neglect terms proportional to C in g [i.e., Eq. (8a)] and P in f [i.e., Eq. (8b)], because they would correspond to degradation leading to damping of the oscillations. The remaining terms on the right-hand side of Eqs. (8a) and (8b) model the feedback loop between Ca^{2+} and IP_3 that produced oscillatory behavior. The primary goal of this analytical study is to identify the resonant conditions that result in symmetry breaking. Oscillatory behavior in composition and not damping is the primary physical phenomenon that is sensitive to resonant interaction with an external oscillatory acoustic stimulus.

In these equations, x marks the position along the one-dimensional tissue and t denotes the time. The first terms in the right-hand side of the Eqs. (8a) and (8b) model the diffusion of Ca^{2+} and IP_3 across the cellular membranes via gap junctions. D_c and D_p are the diffusion coefficients associated with that process. When subjected to irradiation by a sound wave with a frequency Ω and a wave number K, the spatially and temporally varying pressure field will lead to a modulation of the gap-junction cell-to-cell conductance. This modulation is again represented by the spatiotemporal variations of the diffusion coefficients given in Eqs. (7a) and (7b). For the sake of analytical simplicity, we take $D_{1c} = D_{1p} = \varepsilon$, that is, the modulation of cell-to-cell conduction is the same for Ca^{2+} and IP_3 but not necessarily the nonmodulated diffusivities, D_{0c}, D_{0p}. The periodicity of the modulated diffusion coefficients suggests that we should be seeking solutions of Eqs. (8a) and (8b) in the form of Bloch waves:

$$C(x,t) = \sum_k \sum_g C(k,g,t)e^{i(k+g)x}, \tag{9a}$$

$$P(x,t) = \sum_k \sum_g P(k,g,t)e^{i(k+g)x}, \tag{9b}$$

where $x \in [0,L]$. The wave number k is limited to the first Brillouin zone: $[\frac{-\pi}{L}, \frac{\pi}{L}]$ and $g = \frac{2\pi}{L}m$ with m being a positive

or negative integer. With these, Eqs. (2a) and (2b) take the form:

$$\frac{\partial C(k+g,t)}{\partial t} = -(k+g)^2 D_{0c} C(k+g,t) - rP(k+g,t) + \varepsilon[f(k+g-K)e^{i\Omega t}C(k+g-K,t) + h(k+g+K)e^{-i\Omega t}C(k+g+K,t)], \tag{10a}$$

$$\frac{\partial P(k+g,t)}{\partial t} = -(k+g)^2 D_{0p} P(k+g,t) + rC(k+g,t) + \varepsilon[f(k+g-K)e^{i\Omega t}P(k+g-K,t) + h(k+g+K)e^{-i\Omega t}P(k+g+K,t)]. \tag{10b}$$

The functions $f(k)$ and $h(k)$ are defined by $f(k+g) = -(k+g)^2 - K(k+g)$ and $h(k+g) = -(k+g)^2 + K(k+g)$.

For the sake of analytical tractability, we treat ε as a perturbation and use multiple time scale perturbation theory [40] to shed light on the effect of the sound wave on the biological waves. In absence of sound irradiation, $\varepsilon = 0$, the wave behavior of the Ca^{2+} and IP_3 concentration excursions take the form

$$C_0(k+g,t) = a_0\xi(k+g)e^{i\omega_0(k+g)t}, \tag{11a}$$

$$P_0(k+g,t) = (-1)a_0\zeta(k+g)e^{i\omega_0(k+g)t}, \tag{11b}$$

with

$$\xi(k+g) = \sqrt{\alpha \mp i\sqrt{r^2-\alpha^2}}, \tag{12a}$$

$$\zeta(k+g) = \sqrt{\alpha \pm i\sqrt{r^2-\alpha^2}}, \tag{12b}$$

and a dispersion relation

$$\omega_0(k+g) = \pm\omega_r + i\omega_i. \tag{13}$$

In Eqs. (12a), (12b), and (13), we have defined the following quantities: $\alpha = (k+g)^2\frac{(D_{0c}-D_{0p})}{2}$, the real frequency $\omega_r = \sqrt{r^2-\alpha^2}$, and the imaginary part of the frequency $\omega_i = (k+g)^2\frac{(D_{0c}+D_{0p})}{2}$. a_0 is a constant amplitude. The functions ξ and ζ lead to wave-number-dependent phase differences between the oscillations of Ca^{2+} and the oscillations of IP_3. For instance, for a very long wavelength mode $k+g \sim 0$, the Ca^{2+} and IP_3 composition incursions are $\frac{\pi}{2}$ out of phase. The $\pm$ in front of the real part of the frequency of the calcium and IP_3 waves represents two types of solutions that propagate in opposite directions. The imaginary part of the frequency results in the damping of the compositional waves. The multiple-time-scale perturbation approach is carried out to first and second order with details reported in the Appendix. The sound wave is shown to lead to an alteration of the dispersion relation of the Ca^{2+} and IP_3 waves given by Eqs. (11a) and (11b). These alterations occur at wave numbers k' and k'', which satisfy the following equations:

$$\omega_0(k'+g+K) = \omega_0(k'+g) + \Omega, \tag{14a}$$

$$\omega_0(k''+g-K) = \omega_0(k''+g) - \Omega. \tag{14b}$$

The most remarkable result is that while k' and k'' are solutions of (14a) and (14b), $-k'$ and $-k''$ are not. This means that the actual dispersion relation of the Ca^{2+} and IP_3 waves perturbed by the acoustic wave is not symmetrical about the origin $k = 0$. This asymmetry tells us that there exist intervals of frequency and wave numbers whereby the propagation of Ca^{2+} and IP_3 waves in one direction differs from the propagation in the opposite direction. Irradiation by an acoustic wave has broken the directional symmetry of the biological waves, leading to nonreciprocity in the propagation of the intercellular signal. It is worth noting that since the dispersion relation ω_0 could be a reasonably shallow function of k, the resonant conditions (14a) and (14b) may correspond to large values of $k = k'(k'')$ and small values of Ω that do not satisfy the relation $\Omega = ck$. The small value of Ω may be attained by the superposition of counterpropagative acoustic waves with slightly differing frequencies and wave numbers as was discussed in Sec. II A. Equations (14a) and (14b) also provide a physical interpretation of the origin of symmetry breaking in terms of scattering phenomena. Considering Eq. (14a), the acoustic modulation with wave number K scatters a calcium wave with wave number $k'+g$ to produce a calcium wave with wave number $k'+g+K$. This scattering process conserves the wave number. In the absence of symmetry breaking, the scattering cross section for scattering of left-moving and right-moving calcium waves would be equal. However, with the introduction of the acoustic wave, which breaks the time-reversal symmetry, the scattering cross sections are no longer the same. The resulting asymmetry can also be explained within the context of topology, as we discuss next.

The analytical model analyzed herein enables us to shed light on the topology of the calcium wave function in wave number space. The amplitude of the calcium waves changes sign (i.e., accumulates a π geometrical phase [41]) as one is moving along wave number space through the resonant conditions (14a) and (14b) (i.e., through k' and k''). On the other hand, the amplitude is not accumulating any geometric phase along a path in wave number space that goes through $-k'$ and $-k''$. This observation indicates that the manifold in wave number space that supports the calcium wave function exhibits a nonconventional topology. This manifold possesses a twist at k' and k'' but not at $-k'$ and $-k''$, as illustrated schematically in Fig. 3. Parallel transport of a vector field that may represent the wave amplitude along a closed path in k space (here a circle) can be used to describe this topology. The geometrical phase change of the amplitude of the calcium wave is represented by the change in orientation of the vector tangent to the manifold as it is parallel transported along the path. This behavior is phenomenologically equivalent to topological insulators more commonly known in the physical sciences [15–17].

The linear model so far has included advective terms. A simplified version of that model which neglects advection takes the form given by Eqs. (15a) and (15b):

$$\frac{\partial C(x,t)}{\partial t} = D_c(x,t)\frac{\partial^2 C(x,t)}{\partial x^2} - rP(x,t), \tag{15a}$$

$$\frac{\partial P(x,t)}{\partial t} = D_p(x,t)\frac{\partial^2 P(x,t)}{\partial x^2} + rC(x,t). \tag{15b}$$

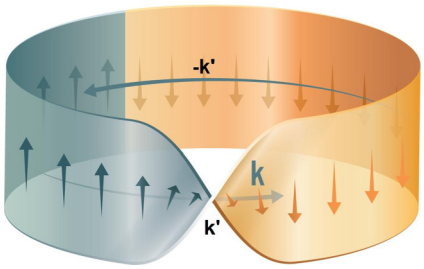

FIG. 3. (Color online) Sound-induced twist in the topology of linear calcium waves. Schematic illustration of the k-space manifold supporting calcium waves in the one-dimensional tissue subjected to acoustic irradiation. The manifold takes the general form of a strip with a single twist centered on the wave number k'. The geometrical phase change π of the amplitude of the wave is represented by the change in orientation of a vector field (arrows) tangent to the manifold as the vector is transported across k'. The amplitude of the calcium wave function does not accumulate a phase across $-k'$. A similar topology is expected at k''.

The treatment of this simplified problem with the multiple time scale perturbation is similar to that presented for the more general case in the Appendix. The major difference lies only in a simplified form of the functions $f(k)$ and $h(k)$, which are now defined by $f(k+g) = -(k+g)^2$ and $h(k+g) = -(k+g)^2$. Neglecting advection is then determined not to affect the observation of symmetry breaking in the direction of propagation.

These results support the observation of symmetry breaking in the direction of propagation of calcium waves observed in the numerical simulation of the nonlinear reaction-diffusion model of Sec. II A.

III. CONCLUSIONS

We investigated the propagation of gap-junction-based intercellular calcium signals in a nonlinear reaction-diffusion model of calcium waves in a one-dimensional tissue subjected to a spatiotemporal modulation of cell-to-cell conductance due to irradiation by an acoustic wave. This numerical model of gap-junction-based calcium wave propagation was employed to capture some of the complexity of intracellular calcium dynamics, particularly, the dynamics of calcium channels in the membrane of the ER. This complex model is formulated into a system of nonlinear coupled differential equations involving four dynamical variables: the concentrations of Ca^{2+} and IP_3 in the cytosol, but also the calcium concentration in the ER stores and the fraction of IP_3 receptors on the ER membrane that have not been inactivated by Ca^{2+}. Irradiation by an acoustic wave is accounted for by considering a spatiotemporal modulation of the Ca^{2+} and IP_3 conductances. Numerical simulations of the nonlinear model with advection and without advection demonstrate symmetry breaking in the direction of propagation of calcium waves and therefore, nonreciprocity in the propagation of gap-junction-based intercellular calcium signals due to sound irradiation.

A simplified linear reaction-diffusion model was used to model the oscillatory dynamics of the excursions in the concentrations of Ca^{2+} and IP_3 about equilibrium by lumping many of the fine-detail control systems of cellular calcium [23] (i.e., regulatory players such as SERCA pumps, G proteins, differentially responding Ca channels) within a single reaction rate constant, r. Similarly to the nonlinear model, the effect of spatially and temporally varying sound pressure was also accounted for via a spatiotemporal modulation of the gap-junction cell-to-cell conductance. In spite of the simplicity of the model, perturbation theory showed analytically the existence of intercellular calcium waves with unidirectional signal propagation. Observation of symmetry breaking in the direction propagation was also obtained whether the model included advection or not. The linear model provided additional information that the numerical model could not, concerning the functional form of the calcium wave under irradiation. The amplitude of the irradiated calcium wave exhibits nonconventional topology with torsional character in wave number space.

In an attempt to generalize the analysis, we have also considered (but not reported here) a linear model system whereby the reaction rate r and not the diffusion coefficients of Ca^{2+} and IP_3 is modulated spatiotemporally. This calculation also showed nonreciprocity in calcium wave propagation. Observation of asymmetric calcium wave propagation in linear model systems with either modulated conductance or intracellular reaction rate suggests that symmetry breaking due to sound irradiation is likely to be insensitive to the details of the biological mechanism that is responsive to the acoustic waves. Since all linear models (i.e., with spatiotemporal modulation of the diffusion coefficient with or without advection, or with spatiotemporal modulation of reaction rate) and the nonlinear models (with advection and without advection) considered in the present study show nonreciprocity in the propagation of calcium waves when subjected to an acoustic wave, it is likely that the phenomenon of symmetry breaking due to sound irradiation exhibits some robustness with respect to the biological complexity of the intercellular and intracellular dynamics.

It is thought that (a) the observation of nonreciprocity in calcium signaling in a realistic nonlinear reaction-diffusion model of calcium waves and (b) the existence of a similar behavior in the simplified linear model of calcium waves should be of some help in interpreting real biological phenomena associated with the beneficial therapeutic effects of sound irradiation but also possibly the harmful effects of sound waves on health. The evaluation of the risks of routine prenatal ultrasound imaging on a fetus during pregnancy has not considered the possible effect on intercellular signaling identified here [42]. It is also known that exposure to traffic noise in addition to that of air pollution leads to an increase in risk of cardiovascular diseases [43,44]. The mechanisms driving the effect of noise exposure on the function of the cardiovascular system are essentially unknown. Finally, vibroacoustic disease (VAD) is a pathology that develops in individuals excessively exposed to low-frequency sound [45]. VAD is associated with the abnormal growth of extracellular matrices (collagen and elastin), in the absence of an inflammatory process, seen in blood vessels, cardiac structures, trachea, lung, and kidney. VAD appears to be a mechano-transduction disease resulting from impairment of mechanically mediated signaling in exposed tissues [45]. The effects of the physical parameters of the sound on signaling, such as frequency or intensity (amplitude), are essentially unknown.

We also note that the observed mechanism of nonreciprocity in the propagation of intercellular calcium signals should be applicable to other types of intercellular signals. Given that our analysis does not depend on the specific chemical species involved in signaling, it is likely that our results apply to other signaling molecules such as oxidizing chemical agents that are thought to play roles similar to calcium in plant cells [46,47].

It is the hope and objective of the authors of the present theoretical and computational study to create awareness and motivate experimental studies of the beneficial or the harmful effects of sound in the context of the essentially unknown phenomenon of nonconventional topology and nonreciprocity of propagation of gap-junction-based intercellular signaling induced by acoustic irradiation.

APPENDIX: MULTIPLE TIME SCALE PERTURBATION THEORY ANALYSIS

For the sake of analytical tractability, we treat ε in Eqs. (10a) and (10b) of the main text as a perturbation and write the concentration excursions C and P as a second-order power series in the perturbation, namely,

$$C(k+g,\,\tau_0,\tau_1,\tau_2) = C_0(k+g,\,\tau_0,\tau_1,\tau_2) + \varepsilon C_1(k+g,\,\tau_0,\tau_1,\tau_2) + \varepsilon^2 C_2(k+g,\,\tau_0,\tau_1,\tau_2), \tag{A1a}$$

$$P(k+g,\,\tau_0,\tau_1,\tau_2) = P_0(k+g,\,\tau_0,\tau_1,\tau_2) + \varepsilon P_1(k+g,\,\tau_0,\tau_1,\tau_2) + \varepsilon^2 P_2(k+g,\,\tau_0,\tau_1,\tau_2). \tag{A1b}$$

In Eqs. (A1a) and (A1b), X_i with $i = 0,1,2$ and $X = C,P$ are the concentrations excursions expressed to zeroth order, first order, and second order in the perturbative time, respectively. Because the sought solution might have several time characteristics, multiple time scale perturbation theory expands the problem onto a series of time scales expressed in powers of the perturbation parameter times time. Considering the problem to second order in perturbation, we have replaced the single time variable t by three variables representing different time scales: $\tau_0 = t$, $\tau_1 = \varepsilon t$, and $\tau_2 = \varepsilon^2 t = \varepsilon^2 \tau_0$. We can subsequently decompose Eqs. (10a) and (10b) into three equations: one equation to zeroth order in ε, one equation to first order in ε, and a third equation to second order in ε. The zeroth-order equation represents the dynamics of Ca^{2+} and IP_3 concentration excursions in the absence of sound irradiation. To zeroth order, the solutions take the form similar to that reported in the main text:

$$C_0(k+g,\tau_0,\tau_1,\tau_2) = a_0^c(\tau_1,\tau_2)\xi(k+g)e^{i\omega_0(k+g)\tau_0}, \tag{A2a}$$

$$P_0(k+g,\tau_0,\tau_1,\tau_2) = (-1)a_0^p(\tau_1,\tau_2)\zeta(k+g)e^{i\omega_0(k+g)\tau_0}, \tag{A2b}$$

with

$$\xi(k+g) = \sqrt{\alpha \mp i\sqrt{r^2-\alpha^2}}, \tag{A3a}$$

$$\zeta(k+g) = \sqrt{\alpha \pm i\sqrt{r^2-\alpha^2}}\,, \tag{A3b}$$

and a dispersion relation

$$\omega_0(k+g) = \pm\omega_r + i\omega_i. \tag{A4}$$

In Eqs. (A3a), (A3b), and (A4), we have defined the following quantities: $\alpha = (k+g)^2\frac{(D_{0c}-D_{0p})}{2}$, the real frequency $\omega_r = \sqrt{r^2-\alpha^2}$, and the imaginary part of the frequency $\omega_i = (k+g)^2\frac{(D_{0c}+D_{0p})}{2}$. To zeroth order, the amplitude functions obey $a_0^c(\tau_1,\tau_2) = a_0^p(\tau_1,\tau_2) = a_0(\tau_1,\tau_2)$; however, we will keep the upper scripts to differentiate between calcium and IP_3 amplitudes, since to higher order in perturbation theory, these quantities may differ.

The first-order equations are used to solve for C_1 and P_1 :

$$\begin{aligned}
&\frac{\partial C_1(k+g,\tau_0,\tau_1,\tau_2)}{\partial\tau_0} + (k+g)^2 D_{0c} C_1(k+g,\tau_0,\tau_1,\tau_2) + r P_1(k+g,\tau_0,\tau_1,\tau_2)\\
&\quad = -\frac{\partial C_0(k+g,\tau_0,\tau_1,\tau_2)}{\partial\tau_1} + f(k+g-K)e^{i[\Omega+\omega_0(k+g-K)]\tau_0}a_0^c(\tau_1,\tau_2)\xi(k+g-K,\tau_1,\tau_2)\\
&\qquad + h(k+g+K)e^{i[-\Omega+\omega_0(k+g+K)]\tau_0}a_0^c(\tau_1,\tau_2)\xi(k+g+K,\tau_1,\tau_2),
\end{aligned} \tag{A5a}$$

$$\begin{aligned}
&\frac{\partial P_1(k+g,\tau_0,\tau_1,\tau_2)}{\partial\tau_0} + (k+g)^2 D_{0p} P_1(k+g,\tau_0,\tau_1,\tau_2) - r C_1(k+g,\tau_0,\tau_1,\tau_2)\\
&\quad = -\frac{\partial P_0(k+g,\tau_0,\tau_1,\tau_2)}{\partial\tau_1} - f(k+g-K)e^{i[\Omega+\omega_0(k+g-K)]\tau_0}a_0^p(\tau_1,\tau_2)\zeta(k+g-K,\tau_1,\tau_2)\\
&\qquad - h(k+g+K)e^{i[-\Omega+\omega_0(k+g+K)]\tau_0}a_0^p(\tau_1,\tau_2)\zeta(k+g+K,\tau_1,\tau_2).
\end{aligned} \tag{A5b}$$

The first term in the right-hand side of these two equations leads to secular solutions and needs to be eliminated. This is achieved by imposing on the zeroth-order solutions, as well as subsequent order solutions, independence of the time scale τ_1. The other right-hand side terms serve as driving forces for the first-order solutions. The solutions of Eqs. (A5a) and (A5b) are therefore the sum of the solutions to the homogeneous solutions (i.e., without the driving force) and of particular solutions. The solutions to the homogeneous equations have forms similar to the solutions given by Eqs. (A2).

The first-order particular solutions take the following form:

$$C_1^{(p)}(k+g,\tau_0,\tau_2) = b_1(k+g)e^{i[\Omega+\omega_0(k+g-k)]\tau_0} + b_1'(k+g)e^{i[-\Omega+\omega_0(k+g+K)]\tau_0}, \tag{A6a}$$

$$P_1^{(p)}(k+g,\tau_0,\tau_2) = d_1(k+g)e^{i[\Omega+\omega_0(k+g-K)]\tau_0} + d_1'(k+g)e^{i[-\Omega+\omega_0(k+g+K)]\tau_0}, \tag{A6b}$$

with

$$b_1(k+g) = \frac{1}{\Delta_1(k+g)}\big[f(k+g-K)a_0^c(\tau_2)\xi(k+g-K)\big\{i[\Omega+\omega_0(k+g-K)] + (k+g)^2 D_{0p}\big\} + rf(k+g-K)a_0^p(\tau_2)\zeta(k+g-K)\big], \tag{A7a}$$

$$b_1'(k+g) = \frac{1}{\Delta_2(k+g)}\big[h(k+g+K)a_0^c(\tau_2)\xi(k+g+K)\big\{i[-\Omega+\omega_0(k+g+K)] + (k+g)^2 D_{0p}\big\} + rh(k+g-K)a_0^p(\tau_2)\zeta(k+g+K)\big], \tag{A7b}$$

$$d_1(k+g) = \frac{1}{\Delta_1(k+g)}\big[-f(k+g-K)a_0^p(\tau_2)\zeta(k+g-K)\big\{i[\Omega+\omega_0(k+g-K)] + (k+g)^2 D_{0c}\big\} + rf(k+g-K)a_0^c(\tau_2)\xi(k+g-K)\big], \tag{A7c}$$

$$b_1'(k+g) = \frac{1}{\Delta_2(k+g)}\big[-h(k+g+K)a_0^p(\tau_2)\zeta(k+g+K)\big\{i[-\Omega+\omega_0(k+g+K)] + (k+g)^2 D_{0c}\big\} + rh(k+g+K)a_0^c(\tau_2)\xi(k+g+K)\big], \tag{A7d}$$

and

$$\Delta_1(k+g) = r^2 + \big\{i[\Omega+\omega_0(k+g-K)] + (k+g)^2 D_{0c}\big\}\big\{i[\Omega+\omega_0(k+g-K)] + (k+g)^2 D_{0p}\big\}, \tag{A8a}$$

$$\Delta_2(k+g) = r^2 + \big\{i[-\Omega+\omega_0(k+g+K)] + (k+g)^2 D_{0c}\big\}\big\{i[-\Omega+\omega_0(k+g+K)] + (k+g)^2 D_{0p}\big\}. \tag{A8b}$$

The conditions $\Delta_1 = 0$ and $\Delta_2 = 0$ lead to resonances.

The second-order equations take the form:

$$\frac{\partial C_2(k+g,\tau_0,\tau_2)}{\partial\tau_0} + (k+g)^2 D_{0c} C_2(k+g,\tau_0,\tau_2) + rP_2(k+g,\tau_0,\tau_2) = -\frac{\partial C_0(k+g,\tau_0,\tau_2)}{\partial\tau_2} + f(k+g-K)e^{i\Omega\tau_0}C_1(k+g-K,\tau_2) + h(k+g+K)e^{-i\Omega\tau_0}C_1(k+g+K\tau_2) \tag{A9a}$$

$$\frac{\partial P_2(k+g,\tau_0,\tau_2)}{\partial\tau_0} + (k+g)^2 D_{0c} P_2(k+g,\tau_0,\tau_2) + rC_2(k+g,\tau_0,\tau_2) = -\frac{\partial P_0(k+g,\tau_0,\tau_2)}{\partial\tau_2} + f(k+g-K)e^{i\Omega\tau_0}P_1(k+g-K,\tau_2) + h(k+g+K)e^{-i\Omega\tau_0}P_1(k+g+K\tau_2) \tag{A9b}$$

The first term in the left-hand side of both equations is proportional to $e^{i\omega_0(k+g)\tau_0}$ and therefore leads to secular behavior. Inserting Eqs. (A6a) and (A6b) into (A9a) and (A9b) leads to additional secular terms. Regrouping these terms and setting them to zero results in the following set of two equations:

$$\frac{\partial a_0^c(\tau_2)}{\partial\tau_2} = a_0^c(\tau_2)F_1(k+g) + a_0^p(\tau_2)F_2(k+g), \tag{A10a}$$

$$\frac{\partial a_0^p(\tau_2)}{\partial\tau_2} = a_0^p(\tau_2)G_2(k+g) + a_0^c(\tau_2)G_1(k+g), \tag{A10b}$$

with

$$F_1(k+g) = \frac{h^2(k+g)}{\Delta_2(k+g-K)}F_p + \frac{f^2(k+g)}{\Delta_1(k+g+K)}G_p,$$

$$F_2(k+g) = r\gamma\left[\frac{h^2(k+g)}{\Delta_2(k+g-K)} + \frac{f^2(k+g)}{\Delta_1(k+g+K)}\right],$$

$$G_1(k+g) = -r\gamma^{-1}\left[\frac{h^2(k+g)}{\Delta_2(k+g-K)} + \frac{f^2(k+g)}{\Delta_1(k+g+K)}\right],$$

$$G_2(k+g) = \frac{h^2(k+g)}{\Delta_2(k+g-K)}F_c + \frac{f^2(k+g)}{\Delta_1(k+g+K)}G_c,$$

and

$$\begin{aligned} F_{p,c} &= i[-\Omega + \omega_0(k+g)] + (k+g-K)^2 D_{0p.c,} \\ G_{p,c} &= i[\Omega + \omega_0(k+g)] + (k+g+K)^2 D_{0p,c}, \\ \gamma(k+g) &= \frac{\zeta(k+g)}{\xi(k+g)} = e^{\pm i\varphi_0}, \\ \gamma^{-1} &= \gamma^* = e^{\mp i\varphi_0}. \end{aligned}$$

We now chose the following forms for the calcium and IP_3 amplitudes $a_0^c(\tau_2) = Ae^{i\delta\tau_2}e^{+i\varphi_2}$ and $a_0^p(\tau_2) = Ae^{i\delta\tau_2}e^{-i\varphi_2}$ such that both amplitudes have the same second-order frequency shift δ but differ in their phase. We saw earlier that to zeroth order in perturbation these amplitudes were identical. However, we kept the upper script c and p throughout our derivation to reflect the possibility of a phase difference φ_2 that arises from carrying the perturbation expansion up to second order. Inserting these forms for the amplitudes into Eqs. (A10a) and (A10b) results in the following corrections to the zeroth-order frequency and phases of the Ca^{2+} and IP_3 waves:

$$\begin{aligned} \omega_0^{\mathrm{cor}}(k+g) = \omega_0(k+g) - \varepsilon^2\Bigg[&\frac{h^2(k+g)}{\Delta_2(k+g-K)}\left\{r\sin(2\varphi_2 \mp \varphi_0) + \frac{i}{2}(F_p + F_c)\right\} \\ &+ \frac{f^2(k+g)}{\Delta_1(k+g+K)}\left\{r\sin(2\varphi_2 \mp \varphi_0) + \frac{i}{2}(G_p + G_c)\right\}\Bigg], \end{aligned} \tag{A11}$$

$$\cos(2\varphi_2 \mp \varphi_0) = -\frac{1}{r}\frac{\left[\frac{h^2(k+g)}{\Delta_2(k+g-K)}(F_p - F_c) + \frac{f^2(k+g)}{\Delta_1(k+g+K)}(G_p - G_c)\right]}{\frac{h^2(k+g)}{\Delta_2(k+g-K)} + \frac{f^2(k+g)}{\Delta_1(k+g+K)}}. \tag{A12}$$

We note that when approaching the resonance conditions $\Delta_1(k+g+K) \to 0$ and $\Delta_2(k+g-K) \to 0$, the phase given by Eq. (A12) does not diverge. The divergence of Eq. (A11) at the two possible resonances is indicative of two significant alterations of the unperturbed dispersion relation of the Ca^{2+} and IP_3 waves that result from the spatiotemporal modulation of the cell-to-cell conductance due to the applied acoustic wave. These alterations occur at wave numbers k' and k'' which satisfy the following equations:

$$\omega_0(k'+g+K) = \omega_0(k'+g) + \Omega, \tag{A13a}$$

$$\omega_0(k''+g-K) = \omega_0(k''+g) - \Omega. \tag{A13b}$$

[1] R. W. Wood and A. L. Loomis, The physical and biological effects of high frequency sound waves of great intensity, Philos. Mag. J. Sci. **4**, 417 (2009).

[2] E. N. Harvey and A. L. Loomis, High frequency sound waves of small intensity and their biological effects, Nature **121**, 622 (1928).

[3] S. Mitragotri, Healing sound: The use of ultrasound in drug delivery and other therapeutic applications, Nature Reviews Drug Discovery **4**, 255 (2005).

[4] J. D. Heckman, J. P. Ryaby, J. McCabe, J. J. Frey, and R. F. Kilcoyne, Acceleration of tibial fracture-healing by non-invasive, low-intensity pulsed ultrasound, J. Bone & Joint Surgery Am. **76**, 26 (1994).

[5] F. Padilla, R. Puts, L. Vico, and K. Raum, Stimulation of bone repair with ultrasound: A review of the possible mechanic effects, Ultrasonics **54**, 1125 (2014).

[6] C. A. Speed, Therapeutic ultrasound in soft tissue lesions, Rheumatology **40**, 1331 (2001).

[7] Y. Tufail, A. Yoshihiro, S. Pati, and W. J. Tyler, Ultrasonic neuromodulation by brain stimulation with transcranial ultrasound, Nat. Protoc. **6**, 1453 (2011).

[8] G. Leinenga and I. Götz, Scanning ultrasound removes amyloid-β and restores memory in an Alzheimer's disease mouse model, Sci. Transl. Med. **7**, 278ra33 (2015).

[9] W. J. Fry, V. J. Wulff, D. Tucker, and F. J. Fry, Physical factors involved in ultrasonically induced changes in living systems: I. Identification of non-temperature effects, J. Acoust. Soc. Am. **22**, 867 (1950).

[10] J. Parvizi, V. Parpura, J. F. Greenleaf, and M. E. Bolander, Calcium signaling is required for ultrasound-stimulated aggrecan synthesis by rat chondrocytes, J. Orthopaedic Res. **20**, 51 (2002).

[11] M. A. Dinno, M. Dyson, S. R. Young, A. J. Mortimer, J. Hart, and L. A. Crum, The significance of membrane changes in the safe and effective therapeutic and diagnostic ultrasound, Phys. Med. Biol. **34**, 1543 (1989).

[12] F. J. Fry, H. W. Ades, and W. J. Fry, Production of reversible changes in the central nervous system by ultrasound, Science **127**, 83 (1958).

[13] K. Sena, S. R. Angle, A. Kanaji, C. Aher, D. G. Karwo, D. R. Sumner, and A. S. Virdi, Low-intensity pulsed ultrasound and cell-to-cell communication in bone marrow stromal cells, Ultrasonics **51**, 639 (2011).

[14] W. J. Tyler, Y. Tufail, M. Finsterwald, M. L. Tauchmann, E. J. Olson, and C. Majestic, Remote excitation of neuronal circuits using low-intensity, low-frequency ultrasound, PLoS ONE **3**, 1 (2008).

[15] M. Z. Hasan and C. L. Kane, Colloquium: Topological insulators, Rev. Mod. Phys. **82**, 3045 (2010).

[16] A. B. Khanikaev, S. H. Mousavi, W-K. Tse, M. Kargarian, A. H. MacDonald, and G. Shvets, Photonic topological insulators, Nature Mater. **12**, 233 (2013).

[17] H. C. Manoharan, Topological insulators: A romance with many dimensions, Nat. Nanotechnol. **5**, 477 (2010).

[18] A. Trewavas, Le Calcium, c'est la vie: Calcium makes waves, Plant Physiol. **120**, 1 (1999).

[19] H. C. Blair, L. J. Robinson, C. L.-H. Huang, L. Sun, P. A. Friedman, P. H. Schlesinger, and M. Zaid, Calcium and bone disease, Biofactors **37**, 159 (2011).

[20] E. Scemes and C. Giaume, Astrocyte calcium waves: What they are and what they do?, Glia **54**, 716 (2006).

[21] A. H. Carnell-Bell, S. M. Finkbeiner, M. S. Cooper, and S. J. Smith, Glutamate induces calcium waves in cultured astrocytes: Long-range glial signaling, Science **247**, 470 (1990).

[22] S. E. Webb and A. L. Miller, Calcium signaling during embryonic development, Nat. Rev. Mol. Cell Biol. **4**, 539 (2003).

[23] L. Leybaert and M. J. Sanderson, Intercellular Ca^{2+} waves: Mechanisms and functions, Physiol. Rev. **92**, 1359 (2012).

[24] I. Bezprozvanny, J. Watras, and B. E. Ehrlich, Bell-shaped calcium-response curves of IP3 and calcium-gated channels from endoplasmic reticulum of cerebellum, Nature (London) **351**, 751 (1991).

[25] G. L. Combettes and L. Leybaert, Calcium dynamics: Spatio-temporal organization from the subcellular to the organ level, Int. Rev. Cytol. **261**, 193 (2007).

[26] E. A. Finch, T. J. Turner, and S. M. Goldin, Calcium as a coagonist of inositol 1,4,5-trisphosphate-induced calcium release, Science **252**, 443 (1991).

[27] W. H. Evans and P. E. M. Martin, Gap junctions: Structure and function (Review), Mol. Membr. Biol. **19**, 121 (2002).

[28] E. Decrock, D. V. Krysko, M. Vinken, A. Kaczmarek, G. Crispino, M. Bol, N. Wang, M. De Bock, E. De Vuyst, C. C. Naus, V. Rogiers, P. Vandenabeele, C. Erneux, F. Mammano, G. Bultynck, and L. Leybaert, Transfer of IP3 through gap junctions is critical, but not sufficient, for the spread of apoptosis, Cell Death Differ. **19**, 947 (2012).

[29] M. A. Turing, The chemical basis of morphogenesis, Phil. Trans. R. Soc. B **237**, 37 (1952).

[30] A. Politi, L. D. Gaspers, A. P. Thomas, and T. Hofer, Models of IP3 and Ca^{2+} oscillations: Frequency encoding and identification of underlying feedbacks, Biophys. J. **90**, 3120 (2006).

[31] S. G. Rhee, Regulation of phosphoinositide-specific phospholipase, C. Annu. Rev. Biochem. **70**, 281 (2001).

[32] A. T. Harootunian, J. P. Kao, S. Parajape, and R. Y. Tsien, Generation of calcium oscillations in fibroblasts by positive feedback between calcium and IP3, Science **251**, 75 (1991).

[33] A. Verkhratsky, R. K. Orkand, and H. Kettenmann, Glial calcium: Homeostasis and signaling function, Physiol. Rev. **78**, 99 (1998).

[34] D. Communi, V. Vanweyenberg, and C. Erneux, D-myo-inositol-1,4,5-trisphosphate 3-kinase A is activated by receptor activation trough a calcium: Calmodulin-dependent protein kinase II phosphorylation mechanism, EMBO J. **16**, 1943 (1997).

[35] M. J. Sanderson, A. C. Charles, S. Boitano, and E. R. Dirksen, Mechanisms and function of intercellular calcium signaling, Mol. Cell. Endocrinol. **98**, 173 (1994).

[36] N. L. Allbritton, T. Meyer, and L. Stryer, Range of messenger action of calcium ion and inositol 1, 4, 5,-trisphosphate, Science **258**, 1812 (1992).

[37] M. J. Berridge, Inositol trisphosphate and calcium signaling, Nature (London) **361**, 315 (1993).

[38] J. Long, P. A. Deymier, K. Runge, and J. B. Hoying, Regulation of the frequency and wavelength of calcium waves propagating in networks on interconnected cells: A simulation study, Trends Cell Mol. Biol. **9**, 19 (2014).

[39] H-B. Zhao and J. Santos-Sacchi, Effect of membrane tension in gap junctional conductance of supporting cells in Corti's organ, J. Gen. Physiol. **112**, 447 (1998).

[40] R. H. G. Helleman and E. W. Montroll, On a nonlinear perturbation theory without secular terms, Physica **74**, 22 (1974).

[41] M. V. Berry, Quantal phase factors accompanying adiabatic changes, Proc. R. Soc. Lond. A **392**, 45 (1984).

[42] J. P. Newnham, S. F. Evans, C. A. Michael, F. J. Stanley, and L. I. Landau, Effects of frequent ultrasound during pregnancy: A randomized controlled trial, Lancet **342**, 887 (1993).

[43] H. Kälsch, F. Hennig, S. Moebus, S. Möhlenkamp, N. Dragano, H. Jakobs, M. Memmesheimer, R. Erbel, K. H. Jöckel, and B. Hoffmann, Are air pollution and traffic noise independently associated with atherosclerosis: The Heinz Nixdorf recall study, Eur. Heart J. **35**, 853 (2014).

[44] M. Sørensen, Z. J. Andersen, R. B. Nordsborg, S. S. Jensen, K. G. Lillelund, R. Beelen, E. B. Schmidt, A. Tjønneland, K. Overvad, and O. Raaschou-Nielsen, Road traffic noise and incident myocardial infarction: A prospective cohort study, PLoS ONE **7**, e39283 (2012).

[45] M. Alves-Pereira and N. A. A. C. Branco, Vibroacoustic disease: Biological effects of infrasound and low-frequency noise explained by mechanotransduction cellular signaling, Prog. Biophys. Mol. Biol. **93**, 256 (2006).

[46] C. L. Vestergaard, H. Flyvbjerg, and I. M. Møller, Intracellular signaling by diffusion: Can waves of hydrogen peroxide transmit intracellular information in plant cells?, Front. Plant. Sci. **3**, 1 (2012).

[47] S. Neill, R. Desikan, and J. Hancock, Hydrogen peroxide signaling, Curr. Opin. Plant Biol. **5**, 388 (2002).